Preparation of Ultrathin Silsesquioxane Nanofilms via Polymer Langmuir−Blodgett Films

Masaya Mitsuishi, Feng Zhao, Yeji Kim, Akira Watanabe, and Tokuji Miyashita*

Institute of Multidisciplinary Research for Advanced Materials (IMRAM), Tohoku University, 2-1-1 Katahira, Aoba-ku, Sendai 980-8577, Japan

Received January 8, 2008. Revised Manuscript Received April 24, 2008

This Article describes a unique approach to building silsesquioxane nanoassemblies based on the Langmuir−Blodgett (LB) technique. Poly(*N*-dodecylacrylamide-*co*-3-methacryloxypropyl-T8-heptatrifluoropropyl (or heptaphenylpropyl) POSS)s (p(DDA/SQ)s) were synthesized through free radical copolymerization using propyl methacrylate-substituted polyhedral oligomeric silsesquioxane (POSS) monomers containing seven nonreactive trifluoropropyl or phenyl groups ($R_7(Si_8O_{12})(CH_2CH_2CH_2OCOCH_3C{=}CH_2)$ (where R is either trifluoropropyl (SQF) or phenyl (SQPh)) and amphiphilic copolymers. The p(DDA/SQ)s formed stable monolayers at the air/water interface. The monolayers were transferred onto solid substrates as Y-type LB films using a vertical dipping method. The polymer LB films had a well-defined layer structure and a surface flatness (rms values < 1 nm in 1 μm^2). The high heat-resistant properties of the p(DDA/SQ) LB films were demonstrated using UV−vis spectroscopic reflectometry and FT-IR. The refractive index and the thickness of the p(DDA/SQ) LB films were measured as functions of temperature. Upon heating, the refractive index of the p(DDA/SQPh) LB films increased from 1.43 (200 °C) to 1.49 (270 °C), whereas that of poly(*N*-dodecylacrylamide) (pDDA) decreased from 1.38 (200 °C) to 1.28 (220 °C), indicating a densely packed configuration of silsesquioxane units in thin films. A control experiment with pDDA LB films showed domain structures at temperatures greater than 200 °C, although the p(DDA/SQ) LB films remained uniform and smooth after heating to 320 °C. This bottom-up approach is promising for coating with organic and inorganic nanomaterials for optoelectric nanodevice applications.

Introduction

Polyhedral oligometric silsesquioxanes (POSSs) are exciting materials with ladder- or cage-type nanostructures.[1–10] Because of their stiffness attributable to the SiO linkages, these three-dimensional organosilicon oligomers are promising materials for applications in optics,[11–13] catalysis,[14] electronics,[15–17] tissue engineering,[1] and coating[18] with high transparency[19] and good thermal[20,21] and mechanical[22–24] stability. Only a few reports describe the organization of POSS at the nanometer-length scale through "bottom-up" approaches,[9,18,25–27] but the issue has been of great interest; control at the nanometer-length scales provides the highest homogeneity, which in turn engenders the highest reproducibility, predictability, and the best opportunity to tailor materials' properties.[9]

A POSS molecule contains organic substituents on its outer surface. Various POSS monomers are commercially avail-

* To whom correspondence should be addressed. E-mail: miya@tagen.tohoku.ac.jp.

(1) Kannan, R. Y.; Salacinski, H. J.; Butler, P. E.; Seifalian, A. M. *Acc. Chem. Res.* **2005**, *38*, 879–884.
(2) Phillips, S. H.; Haddad, T. S.; Tomczak, S. J. *Curr. Opin. Solid State Mater. Sci.* **2004**, *8*, 21–29.
(3) Li, G. Z.; Wang, L. C.; Ni, H. L.; Pittman, C. U. *J. Inorg. Organomet. Polym.* **2001**, *11*, 123–154.
(4) Laine, R. M.; Brick, C.; Roll, M.; Sulaiman, S.; Kim, S. G.; Asuncion, M. Z.; Choi, J.; Tamaki, R. In *Functional Nanomaterials*; Geckeler, K. E., Rosenberg, E., Eds.; American Scientific Publisher: California, 2005; pp 295–316.
(5) Voronkov, M. G.; Lavrentyev, V. I. *Top. Curr. Chem.* **1982**, *102*, 199–236.
(6) Baney, R. H.; Itoh, M.; Sakakibara, A.; Suzuki, T. *Chem. Rev.* **1995**, *95*, 1409–1430.
(7) Provatas, A.; Matisons, J. G. *Trends Polym. Sci.* **1997**, *5*, 327–332.
(8) Loy, D. A.; Shea, K. J. *Chem. Rev.* **1995**, *95*, 1431–1442.
(9) Laine, R. M. *J. Mater. Chem.* **2005**, *15*, 3725–3744.
(10) Marcolli, C.; Calzaferri, G. *Appl. Organomet. Chem.* **1999**, *13*, 213–226.
(11) Watanabe, A.; Miyashita, T. *Chem. Lett.* **2006**, *35*, 1130–1131.
(12) Atkins, G. R.; Krolikowska, R. M.; Samoc, A. *J. Non-Cryst. Solids* **2000**, *265*, 210–220.
(13) Liu, Y. L.; Liu, C. S.; Cho, C. I.; Hwu, M. J. *Nanotechnology* **2007**, *18*, 225701.
(14) Duchateau, R. *Chem. Rev.* **2002**, *102*, 3525–3542.
(15) Lo, M. Y.; Zhen, C. G.; Lauters, M.; Jabbour, G. E.; Sellinger, A. *J. Am. Chem. Soc.* **2007**, *129*, 5808–5809.
(16) Liu, P.; Wu, Y. L.; Li, Y. N.; Ong, B. S.; Zhu, S. P. *J. Am. Chem. Soc.* **2006**, *128*, 4554–4555.
(17) Bao, Z. N.; Kuck, V.; Rogers, J. A.; Paczkowski, M. A. *Adv. Funct. Mater.* **2002**, *12*, 526–531.
(18) Brick, C. M.; Chan, E. R.; Glotzer, S. C.; Marchal, J. C.; Martin, D. C.; Laine, R. M. *Adv. Mater.* **2007**, *19*, 82–86.
(19) Dodiuk, H.; Rios, P. F.; Dotan, A.; Kenig, S. *Polym. Adv. Technol.* **2007**, *18*, 746–750.
(20) Tsuchida, A.; Bolln, C.; Sernetz, F. G.; Frey, H.; Mulhaupt, R. *Macromolecules* **1997**, *30*, 2818–2824.
(21) Xu, H. Y.; Kuo, S. W.; Lee, J. S.; Chang, F. C. *Macromolecules* **2002**, *35*, 8788–8793.
(22) Li, G. Z.; Wang, L.; Toghiani, H.; Daulton, T. L.; Pittman, C. U. *Polymer* **2002**, *43*, 4167–4176.
(23) Pan, G. R.; Mark, J. E.; Schaefer, D. W. *J. Polym. Sci., Part B: Polym. Phys.* **2003**, *41*, 3314–3323.
(24) Zhao, Y. Q.; Schiraldi, D. A. *Polymer* **2005**, *46*, 11640–11647.
(25) Cassagneau, T.; Caruso, F. *J. Am. Chem. Soc.* **2002**, *124*, 8172–8180.
(26) Wu, G. J.; Su, Z. H. *Chem. Mater.* **2006**, *18*, 3726–3732.
(27) Zheng, L.; Hong, S.; Cardoen, G.; Burgaz, E.; Gido, S. P.; Coughlin, E. B. *Macromolecules* **2004**, *37*, 8606–8611.

10.1021/cm800067j CCC: $40.75
Published on Web 06/13/2008

able. Their reactive functionalities make POSS compatible with polymers. The incorporation of POSS derivatives into polymeric materials engenders increases in the glass transition temperature, degradation temperature, oxidation resistance, in addition to improved mechanical properties and reduced flammability. The most noteworthy problem, however, is that POSS tends to segregate and form aggregates,[27,28] causing optical inhomogeneities during film formation and difficulty in handling. An effective approach to assembling POSS uniformly at the nanometer level is to add amphiphilic properties. For example, Deng et al. intensively investigated the monolayer behavior of POSS at the air/water interface.[29] Their results, obtained using Langmuir−Blodgett (LB) multilayer deposition of telechelic poly(ethylene glycol)–POSS amphiphiles,[29,30] suggest the high potential of amphiphilic polymers for construction of organic−inorganic nanobuilding blocks. Nanoscale control of POSS ordering in one, two, and three dimensions is of great importance for better understanding and design of POSS nanobuilding blocks.[27]

We have investigated nanomaterial building blocks using LB technique.[31] Polymer LB films, exemplified by poly(*N*-dodecylacrylamide) (pDDA), showed unique amphiphilic properties capable of forming a highly oriented and densely packed monolayer at the air/water interface; the monolayer is continuous, and intermolecular forces, for example, side chain–side chain as well as hydrogen-bonding interactions, are strong. We recently prepared free-standing polymer nanosheet assembly via LB techniques.[32] The polymer LB films can be handled without solid supports. We have called the polymer LB films consisting of pDDA as polymer nanosheets. For this study, we developed ultrathin amphiphilic polymer films to prepare three-dimensional supramolecular POSS architectures. POSS moieties with different substituents were incorporated in organic polymer chains as comonomers with *N*-dodecylacrylamide, which has excellent LB film formation abilities.[31,33,34] The resulting copolymer was expected to provide stable monolayer formation without POSS aggregation. The monolayer was transferred onto solid substrates using a vertical dipping method. The advantage of this method is that the two-dimensional density of the POSS is controllable by adjustment of the POSS contents in the copolymer and that a uniform nanocoating of POSS can be achieved over the centimeter scale in lateral directions. The surface morphology and thermal properties of the nanofilm, as characterized by AFM and UV−vis spectroscopic reflectometry, will be discussed.

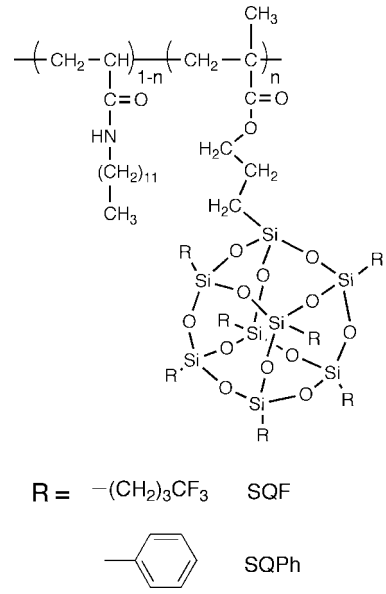

Figure 1. Chemical structure of p(DDA/SQ)s.

Experimental Section

Materials. Comonomers of silsesquioxane derivatives possessing 3,3,3-trifluoropropyl (SQF) or phenyl (SQPh) terminal groups were kindly donated by Chisso Corp. *N*-Dodecylamine, acryloyl chloride, and triethylamine were purchased from Kanto Chemical Co. Inc., Tokyo Chemical Industry Co. Ltd., and Nacalai Tesque Inc., respectively, and used without further purification. Tetrahydrofuran (THF, anhydrous, Aldrich) and acetonitrile (Nacalai Tesque Inc.) were purchased and used without further purification. Toluene, chloroform, and acetone (Kanto Chemical Co. Inc.) were distilled before use. Azobisisobutyronitrile (AIBN; Wako Pure Chemical Industries Ltd.) was recrystallized from methanol. Spectroscopic grade chloroform (Dojindo Laboratories) was used as a spreading solution. Pure distilled water with a resistivity higher than 17.5 MΩ cm (purified by RFD240RA and CPW-101 system; Advantec) was used as the subphase. Octadecyltrichlorosilane (LS-6495, Shin-Etsu Chemical Co. Ltd.) was used without further purification.

Synthesis and Polymerization. The synthesis of *N*-dodecylacrylamide (DDA) has been reported elsewhere.[33,35] Briefly, DDA was synthesized by reacting *N*-dodecylamine with acryloyl chloride in chloroform in the presence of triethylamine as HCl acceptor at ca. 0 °C for 1 h followed by stirring at room temperature for 6 h more. Acryloyl chloride (4.9 mL, 6.0×10^{-3} mol) was added dropwise to the cooled mixture of chloroform (50 mL), *N*-dodecylamine (9.3 g, 5.0×10^{-3} mol), and triethylamine (3.6 mL, 7.1×10^{-3} mol). The resulting mixture was washed sequentially using hydrochloric acid, sodium carbonate, and saturated sodium chloride aqueous solution and then dried using anhydrous sodium sulfate. The crude product was recrystallized from *n*-hexane and dried under vacuum at room temperature.

Copolymers, p(DDA/SQF)s and p(DDA/SQPh)s (Figure 1), were obtained using free-radical polymerization. Comonomers of DDA and SQF or SOPh with AIBN were dissolved in dry THF (p(DDA/SQF)) or toluene (p(DDA/SQPh)). Polymerization was initiated by AIBN at 60 °C for 12 h. In the case of p(DDA/SQF3), for instance, DDA (0.457 g, 1.91×10^{-3} mol), SQF (0.123 g, 1.01×10^{-4} mol), and AIBN (3×10^{-3} g, 1.8×10^{-5} mol) were dissolved in THF (10.2 mL). The solution was subjected to three freeze−thaw cycles to remove oxygen; it was kept at 60 °C for 12 h. The

(28) Kim, G. M.; Qin, H.; Fang, X.; Sun, F. C.; Mather, P. T. *J. Polym. Sci., Part B: Polym. Phys.* **2003**, *41*, 3299–3313.
(29) Deng, J. J.; Polidan, J. T.; Hottle, J. R.; Farmer-Creely, C. E.; Viers, B. D.; Esker, A. R. *J. Am. Chem. Soc.* **2002**, *124*, 15194–15195.
(30) Lee, W.; Ni, S. L.; Deng, J. J.; Kim, B. S.; Satija, S. K.; Mather, P. T.; Esker, A. R. *Macromolecules* **2007**, *40*, 682–688.
(31) Mitsuishi, M.; Ishifuji, M.; Endo, H.; Tanaka, H.; Miyashita, T. *Polym. J.* **2007**, *39*, 411–422.
(32) Endo, H.; Mitsuishi, M.; Miyashita, T. *J. Mater. Chem.* **2008**, 1302–1308.
(33) Miyashita, T.; Mizuta, Y.; Matsuda, M. *Br. Polym. J.* **1990**, *22*, 327–331.
(34) Miyashita, T. *Prog. Polym. Sci.* **1993**, *18*, 263–294.
(35) Arisumi, K.; Feng, F.; Miyashita, T.; Ninomiya, H. *Langmuir* **1998**, *14*, 5555–5558.

Table 1. Characterization of p(DDA/SQ)s

	initial feed	SQ contents (mol %)	M_n	M_w/M_n
p(DDA/SQF3)	95:5	3	6.8×10^3	1.5
p(DDA/SQF7)	90:10	7	7.5×10^3	2.7
p(DDA/SQPh6)	90:10	6	1.5×10^4	2.0
p(DDA/SQPh10)	80:20	10	1.7×10^4	1.7
p(DDA/SQPh22)	70:30	22	1.5×10^4	1.9

copolymers with different mole contents were reprecipitated in acetonitrile from chloroform solutions three times and dried in vacuum overnight at room temperature. The SQ contents were determined using elemental analysis (see Table S1). Molecular weights were determined using gel-permeation chromatography (GPC-8020; Tosoh Corp.) using a polystyrene standard. The mobile phase was THF with a flow rate of 0.6 mL/min. The results are presented in Table 1.

Substrate Preparation. Quartz slides, silicon wafers (p-type; Ryoko Sangyo Corp.), and CaF_2 plates (Pier Optics Co., Ltd.) were used as substrates for LB film deposition. Silicon wafers and quartz slides were freshly cleaned using a UV ozone cleaner, then washed with chloroform and acetone. The substrates were then immersed in a chloroform solution (ca. 1.0×10^{-6} mol/L) of trichlorooctadecylsilane for 12 h. Finally, the substrates were washed with chloroform and dried with flowing nitrogen. The CaF_2 substrates were washed with acetone and chloroform and used without hydrophobic treatment.

LB Film Deposition. A dilute chloroform solution (ca. 1.2×10^{-3} mol/L) of the copolymers was spread onto the water surface. The surface pressure (π)–area (A) isotherms and LB film deposition were carried out using an automatically controlled Langmuir trough (FSD-220 and 21, USI Systems Ltd.). The surface pressure was measured using a paper Wilhelmy plate. The compression rate was 15 cm^2/min. The monolayer was deposited onto the solid substrates using a vertical dipping method with a dipping speed of 10 mm/min, maintaining surface pressure and temperature at 30 mN/m and 15.0 °C, respectively.

Characterization. Film images of p(DDA/SQPh) LB films deposited on silicon wafers were taken using a commercially available digital camera (C-5060; Olympus Corp.). The UV absorption spectra of p(DDA/SQPh) LB films as a function of the number of deposited layers were measured using a spectrophotometer (U-3000; Hitachi Ltd.). X-ray diffraction measurements were carried out with a powder diffractometer ($\lambda = 0.154$ nm (Cu Kα), M18XHF^{22}−SRA; Mac Science Co., Ltd.). The p(DDA/SQPh) LB films with 20 layers were transferred onto glass substrates. Reflected intensities were measured at angle increments of 0.004° from 1° to 10°. The layer spacing of the p(DDA/SQ) LB films was determined from the position of the Bragg peak.

FT-IR Spectra Measurement. Chemical components of p(DDA/SQ) LB films were analyzed using an FT-IR spectrometer (FT/IR4200; Jasco Inc.). The p(DDA/SQ) LB films were transferred onto the CaF_2 substrate at the same deposition conditions described above. The IR spectra of the p(DDA/SQ) LB films were recorded between 4000 and 400 cm^{-1}, with a resolution of 4 cm^{-1} under a continuous nitrogen purge.

AFM Observation. The surface morphology was characterized using atomic force microscopy (SPA400, Seiko Instruments Inc.). A silicon cantilever (14 nN/m and 132 kHz, Si-DFM20, Seiko Instruments Inc.) was used. The images were taken using tapping mode. All measurements were carried out at room temperature unless noted otherwise.

Optical Measurement. The refractive index and thickness of p(DDA/SQ) LB films were determined using in-house UV−vis spectroscopic reflectometry.[36] Briefly, p(DDA/SQ) LB films on silicon wafers were put on the hot stage (HFS91, Linkam Scientific Instruments Ltd.) equipped with an optical microscope (BX-51M; Olympus Corp.). The reflectance spectra were measured using a detection system (CCD camera (DV401, Andor Technology) coupled with a monochromator (MS257, Oriel Instruments)) through a quartz optical fiber. Assuming that the refractive index is described using the Cauchy function, the optical parameters of p(DDA/SQPh) LB films were calculated from the trial values of thickness and model parameters in the Cauchy function using Film Wizard (Scientific Computing International).

Results and Discussion

Monolayer Behavior. The comonomer SQF is dissolved in polar solvents, such as chloroform, acetone, THF, CH_2Cl_2, and DMF, and is not soluble in benzene, toluene, and xylene, although SQPh exhibits better solubility in both polar and nonpolar solvents. The copolymers, p(DDA/SQF)s and p(DDA/SQPh)s, were dissolved in chloroform. The number averaged molecular weight (M_n) and polymer dispersity, the ratio of the weight-averaged molecular weight (M_w) to M_n, are presented in Table 1. All of these copolymers have M_n values between 6.8×10^3 and 1.7×10^4; their corresponding polydispersities are 1.5−2.7.

Figure 2a and b shows π–A isotherms of p(DDA/SQF)s (Figure 2a) and p(DDA/SQPh)s (Figure 2b) measured at 15.0 °C. All p(DDA/SQ) monolayers show a steep rise in surface pressure and high collapsed pressure. The molecularly occupied areas of SQ moieties at the air/water interface were determined from isotherms by extrapolating the linear part of the condensed state in the π–A isotherms to zero pressure. They are presented in Table 2, assuming that the area for the DDA unit is 0.28 nm^2.[34] The SQ area decreases as the SQ content increases. The calculated area of octameric POSS is approximately 1.4 nm^2,[37] indicating that the SQ moieties are located in the hydrophobic side at the air/water interface (Figure 2). Regarding the p(DDA/SQPh) monolayer, the surface limiting area of SQPh moieties decreased as the SQPh content increased. The phenyl rings in SQPh moieties might undergo intermolecular interdigitation because of π–π interaction of phenyl rings.[38] Using these results, the two-dimensional surface density of SQPh was calculated as 5.4×10^{13} cm^{-2} for the p(DDA/SQPh22) monolayer. In other words, the distance of separation between the adjacent SQPh units was determined as 1.5 nm, indicating a densely packed SQPh monolayer formation.

It is noteworthy that the p(DDA/SQF7) monolayer was less stable; a gradual decrease in the surface area was observed when the surface was kept at the surface pressure of 20 mN/m. Probably, multiple fluorinated terminal sites around the cubic core do not contribute to lateral interaction between SQF groups for the stable monolayer formation

(36) Urbanek, M.; Spousta, J.; Navratil, K.; Szotkowski, R.; Chmelik, R.; Bucek, M.; Sikola, T. *Surf. Interface Anal.* **2004**, *36*, 1102–1105.
(37) Laine, R. M.; Brick, C.; Roll, M.; Sulaiman, S.; Kim, S. G.; Asuncion, M. Z.; Choi, J.; Tamaki, R. *Functional Nanomaterials*; American Scientific Publisher: California, 2005.
(38) Strachota, A.; Whelan, P.; Kriz, J.; Brus, J.; Urbanova, M.; Slouf, M.; Matejka, L. *Polymer* **2007**, *48*, 3041–3058.

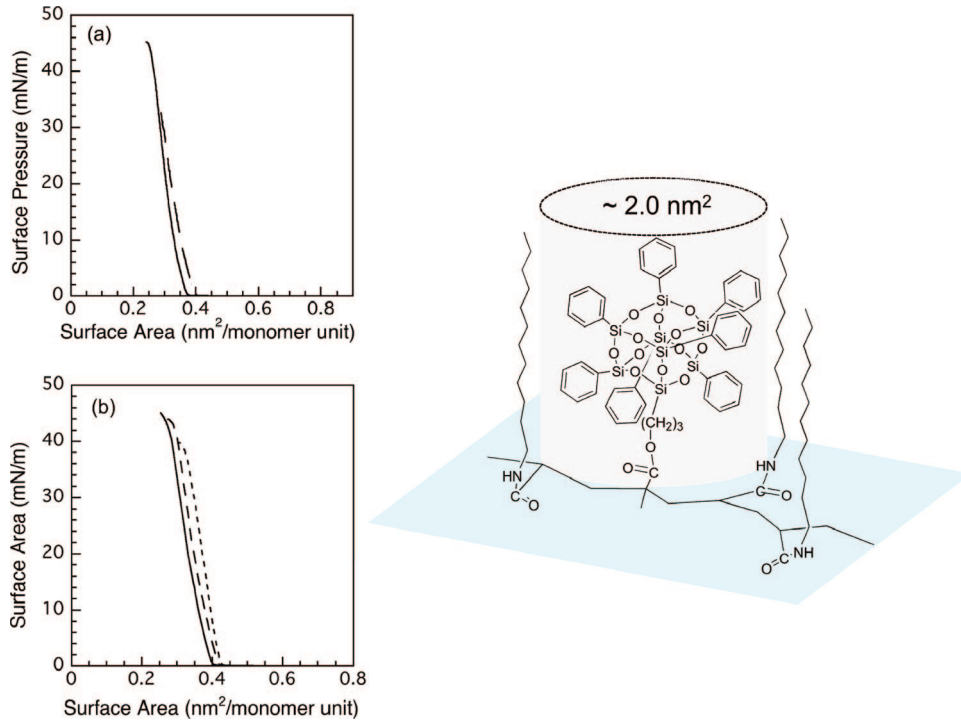

Figure 2. (a) Surface pressure (π)–area (A) isotherms for (a) p(DDA/SQF3) (–) and p(DDA/SQ7) (– – –) and (b) p(DDA/SQPh6) (–), p(DDA/SQ10) (– – –), and p(DDA/SQ22) (- - -) at 15.0 °C. (right) Schematic illustration of p(DDA/SQPh) monolayer at the air/water interface.

Table 2. Monolayer Properties of p(DDA/SQ) LB Films

sample code	cross-sectional area of SQ (nm^2/monomer unit)	transfer ratio		monolayer thickness (nm)
		up	down	
p(DDA/SQF3)	2.28	0.9	0.93	1.63
p(DDA/SQF7)	1.71			
p(DDA/SQPh6)	1.91	1.01	0.94	1.78
p(DDA/SQPh10)	1.28	0.93	0.86	1.79
p(DDA/SQPh22)	0.85	0.91	0.83	1.74

because of their weak hydrophobic interactions.[39,40] The π–A isotherms were also measured as a function of temperature; the collapse pressure decreased as the temperature increased (see Figure S1). As with low molecular weight fatty acids,[41] reducing the temperature tends to make the copolymer monolayer film more coherent and ordered, resulting in reproducible LB film deposition at lower temperatures. All p(DDA/SQ) monolayers, with the exception of p(DDA/SQF7), were transferred onto solid substrates as Y-type LB films with a transfer ratio of almost unity.

p(DDA/SQ) LB Films. The layer structure of p(DDA/SQ)s was confirmed using XRD measurements (Figure 3). As an example, Figure 3 shows an XRD pattern for 20-layer p(DDA/SQF3) LB films. Both Kiessig and Bragg peaks are visible, indicating a highly ordered periodic layer structure and smooth surface. The Bragg peak corresponds to bilayer periodicity for p(DDA/SQF3) LB films, resulting in 1.67 nm monolayer thickness. The 20-layer p(DDA/SQPh) LB films showed a similar tendency, thereby determining the monolayer thickness, 1.78, 1.79, and 1.74 nm, respectively, for p(DDA/SQPh6), p(DDA/SQPh10), and p(DDA/SQPh22) LB films (Table 2). Uniform LB film deposition was confirmed using UV absorption spectra (Figure 4). The absorbance increased linearly with the number of deposited layers, indicating the regular deposition of the p(DDA/SQ) LB films. Although the p(DDA/SQPh) LB films have an absorption band at 250 nm attributable to the π–π^* transition of the phenyl ring, the polymer LB films are optically transparent greater than 300 nm; the transmittance was greater than 90%. Furthermore, these p(DDA/SQ) LB films were transferred onto the solid substrates even at thicknesses of greater than 400 layers.

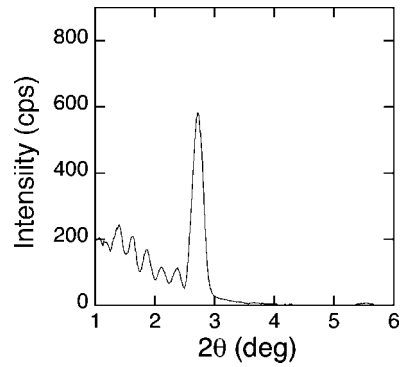

Figure 3. X-ray diffraction patterns for 20-layer p(DDA/SQF3) LB films on a glass substrate.

Figure 5 shows photoimages of p(DDA/SQPh) LB films deposited on silicon wafers. All images were taken at room temperature after maintaining the temperature at the respective temperatures portrayed in Figure 5 for 10 min. They show beautiful interference colors depending on the number of deposited layers. The change in color of p(DDA/SQPh10) LB films shows a tendency identical to that of p(DDA/

(39) Li, X. D.; Aoki, A.; Miyashita, T. *Macromolecules* **1997**, *30*, 2194–2196.
(40) Aminuzzaman, M.; Kado, Y.; Mitsuishi, M.; Miyashita, T. *Polym. J.* **2003**, *35*, 785–790.
(41) Gaines, G. L., Jr. *Insoluble Monolayers at Liquid-Gas Interfaces*; Interscience Publishers: New York, 1966.

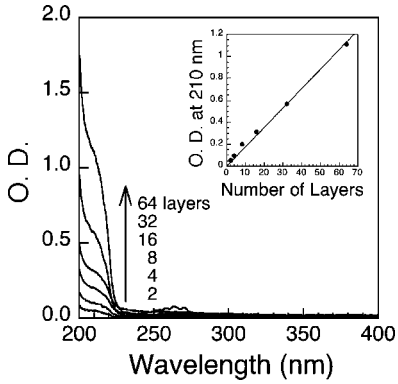

Figure 4. UV absorption spectra of p(DDA/SQPh) LB films as a function of the number of deposited layers.

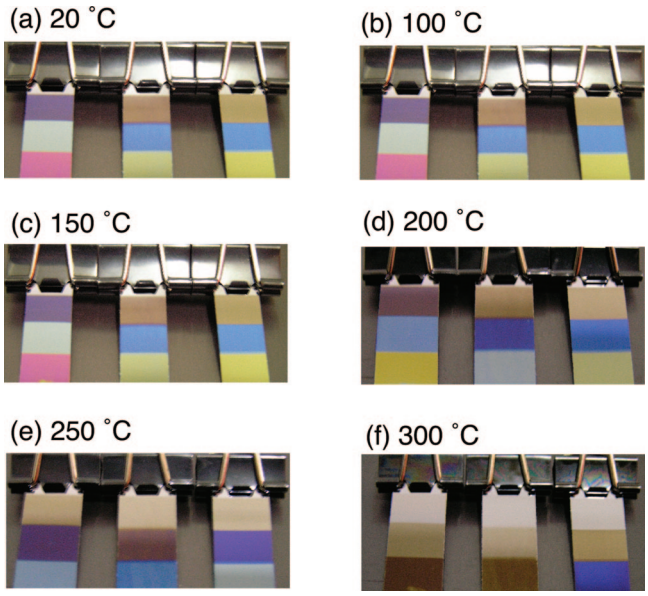

Figure 5. Photograph of p(DDA/SQPh) LB films on silicon wafers with thermal treatments. In each image (from top to bottom), 30, 60, and 90 layers and (from left to right) 6, 10, and 22 mol % SQPh contents.

SQPh22) LB films, whereas p(DDA/SQPh6) LB films show red-shifted colors. The transfer ratio of p(DDA/SQPh) LB films decreases as the SQPh contents increase (Table 2). Probably, the total thickness will decrease as the number of deposited layers increases to over 20 layers with the higher SQPh contents because the SQPh moieties have no LB film formation capability. Interestingly, the decline in thickness seems to be suppressed as the SQPh contents increase. This finding implies that the thermal stability is improved by incorporation of SQPh in the polymer LB films. We failed to obtain the LB films of SQPh homopolymer with high quality. The SQPh homopolymer will take three-dimensional aggregates at the air/water interface. The SQ moieties are probably incorporated as side chains of p(DDA/SQ) and are multilayered by polymer LB film formation. The surface morphology shows good surface flatness [root-mean-square (rms) 0.4 nm in 1 μm × 1 μm] and uniform distribution of SQ moieties in the p(DDA/SQ) LB films, as characterized by AFM (Figure 6). As compared to the surface roughness of nanobuilding blocks via layer-by-layer assembly,[26] the rms value of p(DDA/SQPh) LB films is about one-tenth smaller, indicating that the SQPh units are distributed

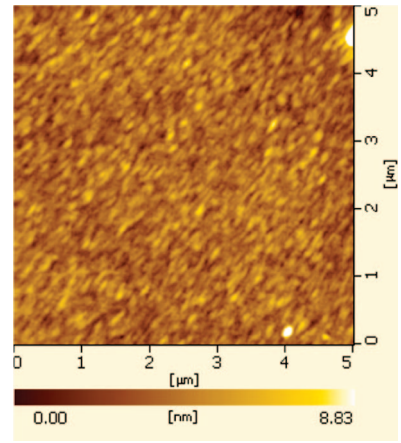

Figure 6. Tapping-mode AFM images of p(DDA/SQPh22) LB films.

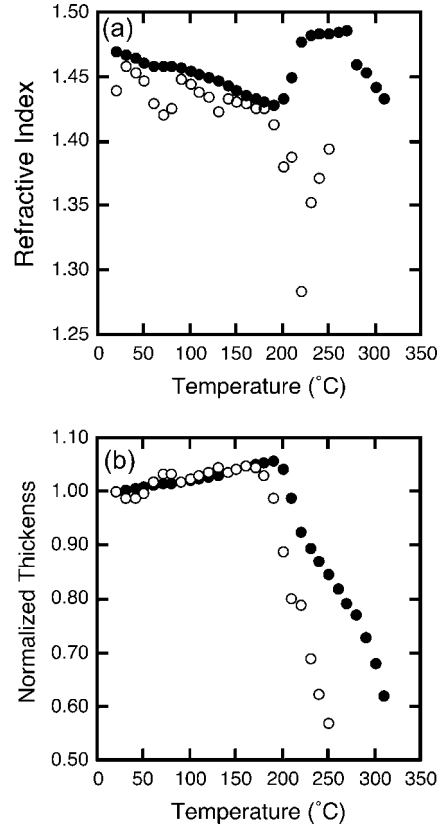

Figure 7. Temperature dependence of (a) refractive index and (b) thickness of 150-layer pDDA (○) and p(DDA/SQPh22) (●) LB films. The film thickness in (b) was normalized with respective thicknesses at room temperature.

uniformly in the polymer LB films without remarkable aggregate formation. We infer that the polymer LB film is a good template for POSS nanobuilding blocks.

Optical and thermal properties of p(DDA/SQPh) LB films were characterized using in situ UV−vis interference patterns. The refractive index and the film thickness of p(DDA/SQPh22) LB films were determined as a function of temperature (Figure 7a and b). Figure 7a shows the refractive index of p(DDA/SQPh22) LB films at 632.8 nm, obtained by fitting. As the temperature increased, the refractive index of pDDA decreased, undergoing complicated up-and-down behavior. Interestingly, the refractive index of p(DDA/SQPh22) LB films increased at temperatures greater than

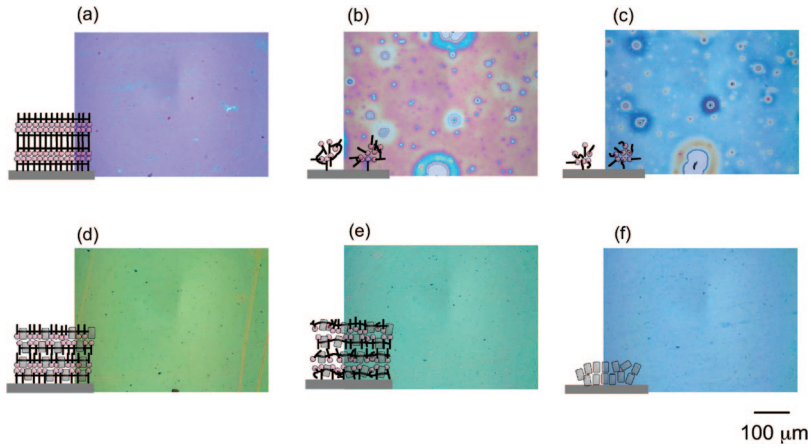

Figure 8. Optical micrograph of (top) 50-layer pDDA and (bottom) 50-layer p(DDA/SQPh22) LB films (150 layers) taken at (a) 20 °C, (b) 200 °C, (c) 30 °C after cooling from 250 °C, and at (d) 20 °C, (e) 200 °C, and (f) 30 °C after cooling from 320 °C. The scale bar corresponds to 100 μm. The schematic illustration shows the layer structure of the polymer LB films.

200 °C. In general, the refractive index of POSS decreases as the curing temperature increases.[42,43] The refractive index of octaphenyl silsesquioxane is 1.56,[12,44] which is larger than that of pDDA (ca. 1.47) because of the high polarizability of phenyl groups (π-bonding electrons). Therefore, the refractive index of p(DDA/SQPh) LB films increased as the SQPh units became closely packed after decomposition of DDA units at temperatures greater than 200 °C. As portrayed in Figure 7b, the film thickness of p(DDA/SQPh22) LB films decreased abruptly at temperatures greater than 200 °C, indicating decomposition of the DDA groups. The thickness of pDDA LB films decreased at temperatures greater than 170 °C. It is noteworthy that the decomposition temperature of p(DDA/SQPh22) LB films is approximately 30 °C higher than that of pDDA LB films. The difference in thermal stability is noticeable using optical microscopy (Figure 8). We took photographs of the pDDA and p(DDA/SQPh22) LB films (50 layers) at 20 °C (Figures 8a and d) and 200 °C (Figure 8b and e), increasing the temperature. Next, we increased the temperature to 250 °C (pDDA) and 320 °C (pDDA/SQPh22)), and finally decreased the temperature to 30 °C (Figures 8c and f). In the case of pDDA LB films, the LB films showed a domain structure at 200 °C (Figure 8b), whereas the p(DDA/SQPh22) LB films retained uniform surface morphology even after cooling the temperature from 320 °C (Figure 8f). Figure 9 shows FT-IR spectra of 50-layer p(DDA/SQPh) LB films upon heating. Briefly, the p(DDA/SQPh22) LB films were transferred onto a CaF_2 substrate; the IR spectra were measured at ambient temperature after the sample was kept at a designated temperature for 10 min. It is noteworthy that the p(DDA/SQPh22) LB films were transferred without hydrophobic treatment of CaF_2 substrates, although the reason remains unclear. The absorption bands at 998 and 1029 cm^{-1}, 1134−1107 cm^{-1}, and 2920 and 2853 cm^{-1} are assigned respectively to C−H stretching and breathing of phenyl ring, asymmetric Si-O-Si stretching, and CH-stretching for DDA (Table 3). The C-H stretching band (ca. 2900 cm^{-1}) decreased abruptly at 200 °C and finally disappeared at 300 °C, although the SQPh units remain on the substrate. These results coincide qualitatively with that of optical microscopic observation. These p(DDA/SQPh) materials show high thermal stability in bulk (see Figure S2). The existence of SQPh unit (decomposition temperature 550 °C)[4] improves the decomposition temperatures of the polymer LB films. The lack of a remarkable shift in wavenumber for Si−O stretching suggests that the SQPh units undergo no chemical reaction, for example,

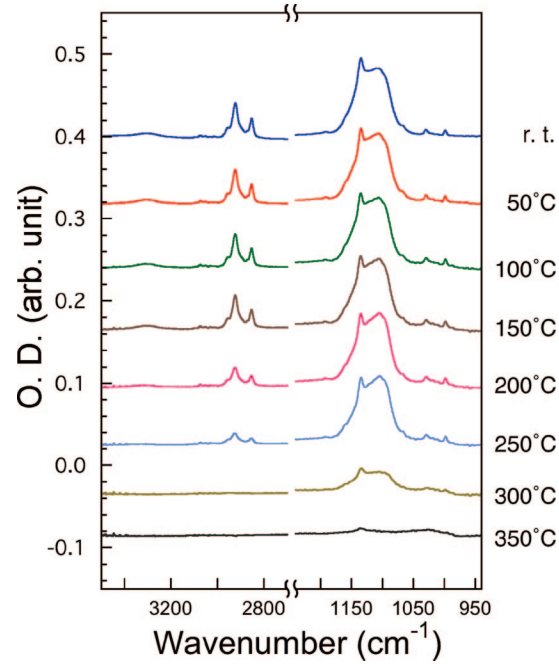

Figure 9. FT-IR spectra of p(DDA/SQPh22) LB films on heating process. For details, see the text.

Table 3. Assignments of Infrared Bands for p(DDA/SQPh) LB Films

wavenumber (cm^{-1})	group	assignments
3307	N−H	stretching
2920	ester C=O	stretching
2853	Si−C_6H_5	bending
1134−1107	Si−O−Si cage	stretching
1029	C−H of phenyl	symmetric stretching
998	phenyl ring	breathing

(42) Yu, S. Z.; Wong, T. K. S.; Hu, X.; Pita, K. *Chem. Phys. Lett.* **2003**, *380*, 111–116.
(43) Yang, C. C.; Chen, W. C. *J. Mater. Chem.* **2002**, *12*, 1138–1141.
(44) Hasui, K.; Tomiki, M.; Okamoto, N. *Jpn. J. Appl. Phys., Part 1* **2004**, *43*, 2341–2345.

network structure formation between SQPh units, as is evident for thermal curing of hydrogen silsesquioxane[45] and hydrogen methyl silsesquioxane.[42] The remaining film, however, was not soluble in chloroform. The slight change in the ratio of Si−O stretching (O.D.(1134 cm^{-1})/O.D.(1104 cm^{-1})) implies the possibility of network formation in the p(DDA/SQPh22) LB films,[42] although the extent of the network formation is not so critical.

Conclusions

In conclusion, hybrid inorganic−organic materials containing silsesquioxane (SQ) were manipulated using Langmuir−Blodgett techniques. The SQ units were distributed uniformly in the polymer LB films. The surface densities of SQ units were calculated as 5.4×10^{13} cm^{-2} for the p(DDA/SQPh22) monolayer, indicating that the SQ units were separated using an averaged center-to-center distance of 1.5 nm. The films show a well-defined layer structure (ca. 3.4 nm bilayer periodicity) and surface smoothness (0.4 nm at 1 μm^2) as well as high LB film deposition capability (ca. 400 layers).

Finally, this study demonstrates that the polymer LB film can serve as a versatile template in which nanomaterials are distributed uniformly without any remarkable aggregation. Further investigation, particularly addressing the processability of p(DDA/SQ) LB films using photochemical reactions as well as thermal treatments, will offer exciting opportunities as a next generation nanomaterial. That work is now in progress.

Acknowledgment. We thank Prof. Hidetoshi Oikawa of IMRAM, Tohoku University, for the use of XRD instruments and Mr. Shohei Tadenuma for technical assistance. We also thank Chisso Corp. for supplying SQ monomers. This work was supported by Grants-in-Aid for Scientific Research ((S) No. 17105006) and for Young Scientists ((A) No. 18685027) from JSPS. This work was partially supported by the Special Education and Research Expenses from the Ministry of Education, Culture, Sports, Science and Technology.

Supporting Information Available: Elemental analysis of p(DDA/SQ)s, π–A isotherms, and thermal analysis of p(DDA/SQPh)s (PDF). This material is available free of charge via the Internet at http://pubs.acs.org.

CM800067J

(45) Siew, Y. K.; Sarkar, G.; Hu, X.; Hui, J.; See, A.; Chua, C. T. *J. Electrochem. Soc.* **2000**, *147*, 335–339.